Substrate-Dependent Morphology of Supramolecular Assemblies: Fibrillin and Type-VI Collagen Microfibrils

Michael J. Sherratt,* David F. Holmes,* C. Adrian Shuttleworth,* and Cay M. Kielty†
*Wellcome Trust Centre for Cell-Matrix Research, School of Biological Sciences, and †School of Medicine, University of Manchester, Manchester, M13 9PT, United Kingdom

ABSTRACT Substrate hydrophobicity/hydrophilicity has previously been shown to affect the morphology and biological function of isolated proteins. We have employed atomic force microscopy to investigate substrate dependent morphologies of two biochemically distinct native supramolecular assemblies: fibrillin and type-VI collagen microfibrils. These morphologically heterogeneous microfibrillar systems are found in many vertebrate tissues where they perform structural and cell-signaling roles. Fibrillin microfibrils adsorbed to a hydrophilic mica substrate adopted a diffuse morphology. Fibrillin microfibrils adsorbed to mica coated with poly-L-lysine or to borosilicate glass substrates had a more compact morphology and a directional asymmetry to the bead, which was not present on mica alone. Intermediate morphologies were observed along a substrate gradient. The classical double-beaded appearance of type-VI collagen microfibrils was evident on mica coated with poly-L-lysine and on glass. On hydrophilic mica, morphology was severely disrupted and there was a major conformational reorganization along the whole collagen microfibril repeat. These observations of substrate dependent conformation have important implications for the interpretation of data from in vitro protein interaction assays and cellular signaling studies. Furthermore, conformational changes may be induced by local charge environments in vivo, revealing or hiding binding sites.

INTRODUCTION

Most microscopical techniques capable of imaging isolated supramolecular assemblies require adsorption of the assembly on substrates such as mica or carbon films. Many biochemical and cell biology techniques for investigating protein-protein and protein-cell interactions also require adsorption of the protein on substrates such as uncoated, poly-L-lysine coated or irradiated plastics. It is thought that structural rearrangements play a crucial role in protein adsorption to substrates (Haynes and Norde, 1995) and that in physiological environments many processes, such as those occurring at the cell surface, are dependent on interfacial phenomena (Kowalewski and Holtzman, 1999). These substrate interactions have the potential to induce conformational changes in adsorbed proteins (Haynes and Norde, 1995), which can affect biological function (Grinnell and Feld, 1981; Garcia et al., 1999; Keselowsky et al., 2003).

Physisorption of proteins to substrates is driven by van der Waals forces, the electrostatic double-layer (EDL) force and the hydrophobic effect (Muller et al., 1997). The van der Waals force can be either attractive or repulsive and the magnitude of the force is dependent on the geometry of the interacting features (Leckband, 2000). The EDL force is dependent on the concentration and valency of charged solutes and the surface charge density of both substrate and protein (Muller et al., 1997). Hydrophobic effects are thought to provide the dominant driving force for the folding of globular proteins in solution where hydrophobic side groups tend to be buried in the interior and hydrophilic side groups are usually located on the periphery of the protein (Haynes and Norde, 1995). The adsorption of proteins to solid surfaces (particularly hydrophobic surfaces) may involve the formation of a water-free contact layer where the protein can unfold without solvating all of its hydrophobic residues (Haynes and Norde, 1995). Substrate hydrophobicity/hydrophilicity has been shown to affect the morphology and/or biological function of adsorbed synthetic and biological macromolecules. The height of adsorbed synthetic ethylenediamine core poly(amidoamine) dendrimers approached the theoretical sphere diameter on hydrophobic but not hydrophilic substrates (Betley et al., 2001). On hydrophilic mica, Alzheimer's β-amyloid peptide formed particulate, pseudomicellar aggregates, but on hydrophobic graphite the same protein organized into uniform, elongated sheets (Kowalewski and Holtzman, 1999).

Substrate dependent morphologies and functions have also been demonstrated for some mammalian extracellular matrix (ECM) proteins. Recombinant human elastin peptides coacervate in heated solutions to form fibrillar aggregates (Bellingham et al., 2001). In an atomic force microscopy (AFM) study these elastin peptides adsorbed to a hydrophilic surface as discrete, rounded aggregates but on a hydrophobic surface the peptides self-assembled into an energetically favorable hexagonally closed packed fibril arrangement (Yang et al., 2002). Fibronectin is an important modular ECM protein, which binds to integrins, collagen, heparan sulfate, hyaluronic acid, and itself. The binding of integrins to surface-bound fibronectin is dependent on the hydrophilicity/hydrophobicity of the surface. Substrate-specific conformational changes have been inferred from solid-phase cell binding assays (Grinnell and Feld, 1981; Garcia et al.,

Submitted September 3, 2003, and accepted for publication January 29, 2004.

Address reprint requests to Michael J. Sherratt, Tel.: +44-161-275-7054; Fax: +44-161-275-5082; E-mail: michael.sherratt@man.ac.uk.

0006-3495/04/05/3211/12 $2.00

1999) and demonstrated for adsorbed fibronectin by AFM (Bergkvist et al., 2003).

Although substrate-dependent morphologies have been observed for some isolated proteins, these effects have not been described for the functional supramolecular assemblies formed by most ECM components. Fibrillin microfibrils and type-VI collagen microfibrils are two biochemically distinct ECM supramolecular assemblies, which interact with cells and other ECM components in vitro and in vivo (Kielty et al., 2002a; Baldock et al., 2003). The interest in fibrillin microfibril biology has been driven by the need to understand the fundamental mechanisms of tissue elasticity and the basis of genotype-to-phenotype correlations in heritable connective tissue diseases such as Marfan syndrome, which are caused by mutations in fibrillin genes (Robinson and Godfrey, 2000). Type-VI collagen microfibrils are found in most vertebrate tissues where they form an extensive microfibrillar network linking cells and many ECM components and maintaining the integrity of tissues such as blood vessels, lung, and skin (Kielty and Grant, 2002).

There is a pressing need to understand the effect of substrate on the conformation of native supramolecular assemblies to aid in the interpretation of solid-phase binding assay data and to gain insights into possible local charge environment dependent conformational switches in vivo. In this study, AFM in ambient conditions has been used to determine the influence of substrate on the conformation of isolated fibrillin and type-VI collagen microfibrils. We report marked substrate-dependent changes that have implications for functional analyses and provide new insights into microfibril supramolecular conformation.

MATERIALS AND METHODS

Materials

Adult bovine eyes and second trimester foetal calves were obtained from the local abattoir within 1 h of death. Bacterial collagenase (type 1A), hyaluronidase (Enzyme Commission, 3.2.1.36) (type X from leech), phenylmethylsulfonyl fluoride (PMSF), *N*-ethylmaleimide (NEM), poly-L-lysine (PLL) (mol wt 70,000–150,000) and 5 nm and 10 nm gold colloids were obtained from Sigma-Aldrich (Poole, Dorset, UK). All other reagents were of analytical grade. Sepharose CL-2B was supplied by Pharmacia-LKB (Milton Keynes, Bucks, UK). Muscovite mica, borosilicate glass coverslips, and electron microscopy grids were obtained from Agar Scientific (Stansted, Essex, UK). Metal support stubs and Olympus high aspect ratio etched silicon probes (spring constant of 42 N m^{-1}) were obtained from Veeco Instruments (Santa Barbara, CA).

Sample and substrate preparation

Adult bovine ciliary zonule and foetal bovine nuchal ligament microfibrils were isolated in native nondenaturing conditions by bacterial collagenase digestion and size exclusion chromatography using modifications of a previously described methodology (Kielty et al., 1991; Wess et al., 1998). Briefly, tissue was incubated with 0.5 mg/ml collagenase, hyaluronidase (final concentration, 5 units/ml), freshly prepared protease inhibitors (2 mM PMSF, 5 mM NEM), and 10 mM $CaCl_2$ in column buffer (400 mM NaCl, 50 mM Tris-HCl, pH 7.4) for 18 h at 4°C. Samples were subsequently centrifuged at 5,000 g for 5 min, and the supernatant was size fractionated on a Sepharose CL-2B column in column buffer. The excluded volume (Vo) of ciliary zonule digests contained abundant fibrillin microfibrils. The excluded volume of nuchal ligament digests contained abundant fibrillin and type-VI collagen microfibrils.

Crosses were scored onto metal sample stubs using a single-edged razor blade. Trimmed mica sheets were adhered to the sample stubs using clear nail varnish. Cleaved mica surfaces were prepared immediately before use by peeling off the top layer of mica with adhesive tape. PLL-coated mica (mica-PLL) was prepared by 2-min incubations with 80 μl 0.01% w/v PLL, followed by three consecutive washes with 300 μl distilled H_2O. Excess liquid was removed from the surface by capillary action at the edge, and the sample was allowed to air dry in a dust-free environment for 30 min before microfibril deposition. Glass coverslips were washed with ethanol followed by distilled H_2O and allowed to air dry for 30 min before sample adsorption. Aliquots of microfibril-containing Vo were diluted 1:8 with column buffer. A sufficient volume of the diluted sample was pipetted onto the substrate and incubated for 1 min before three consecutive washes with 300 μl distilled H_2O. Excess liquid was removed by capillary action and the prepared samples were allowed to air dry overnight in a dust-free environment before microscopical analysis.

The mica to mica-PLL substrate gradient was prepared using a freshly cleaved mica surface adhered to a sample stub marked with a central cross and radii marked at 1000-μm intervals. A 10-μl drop of PLL was pipetted onto the center of the cross, incubated for 2 min, washed three times with 300 μl distilled H_2O, and air dried for 30 min. A sufficient volume of 10% v/v colloidal gold suspension was incubated on the substrate for 10 min before washing as previously described and air drying for 30 min. A sufficient volume of 1:8 dilution ciliary zonule Vo was incubated on the substrate for 1 min before washing and air drying overnight in a dust-free atmosphere.

AFM and image analysis

Samples were imaged by intermittent contact mode in air using a Multimode AFM with a Nanoscope IIIa controller and an E scanner (Veeco Instruments). The Nanoscope optical viewing system was used to aid laser alignment on the cantilever and to locate the cantilever in relation to the cross scored on the metal sample stub. The optical viewing system was calibrated using an electron microscope grid with 45 μm $\times$ 45 μm holes. Cantilever oscillation frequencies and drive amplitudes were determined by the Nanoscope software. Height images were captured at a scan rate of 1.2 Hz and scan sizes of 5, 3, 2.5, 2, or 1 μm. The set point was adjusted to just below the point at which tip-sample interaction was lost. The instrument was calibrated periodically using a grating with 180-nm deep, 10 μm $\times$ 10 μm depressions and during scans with 5 or 10 nm colloidal gold particles. All images were captured at a relative humidity of 30% $\pm$ 5%.

All measurements were conducted on height data, which was first-order flattened using the Nanoscope software. Curved filaments were straightened using the public domain program ImageJ (National Institutes of Health; available on the internet at http://rsb.info.nih.gov/ij/) and the straighten plug-in that fits a nonuniform cubic spline to user-supplied points (Kocsis et al., 1991). Extracted regions were scaled and axial height profiles determined using routines written in Microsoft Visual Basic 6.0 (Redmond, WA). Periodicity determinations were calculated from WSxM developer version 8.0 (Nanotec Electronica, Madrid, Spain; available on the internet at http://www.nanotec.es/). Power spectral analyses of type-VI collagen microfibril periodicities were performed on axial height profiles using WSxM. Roughness analyses (root mean square (RMS)) of PLL to mica binding were carried out with Microsoft Visual Basic 6.0 routines that used the equation employed by the Nanoscope software (Eq. 1) where Z_{ave} is the average Z-value within a given area, Z_i is the current Z-value and N is the number of points within the given area.

$$RMS = \left(\sum (Z_i - Z_{ave})^2 / N\right)^{0.5}. \quad (1)$$

Substrate characterization

Mica, mica-PLL, and glass surface topologies were characterized by AFM. On some substrates RMS roughness values have been shown to be dependent on the measurement area (Long and Chen, 2001). RMS roughness values were calculated for a range of areas (linear dimensions from 31.25 nm × 31.25 nm to 1000 nm × 1000 nm) for 2 μm × 2 μm scans on each substrate, in triplicate.

The binding kinetics of PLL to freshly cleaved mica were investigated over a 32-min time course at time points of 0, 1, 2, 4, 8, 16, and 32 min. RMS values, of mica, mica-PLL, and glass, were calculated for 60 (105 × 105 nm) areas randomly placed over three 2 μm × 2 μm scans. The percentage coverage of PLL on the mica surface was calculated by autothresholding in ImageJ.

Mica, mica-PLL, and glass substrate hydrophobicity/hydrophilicity was quantified by measuring the drop contact angle (θ), formed between the liquid-vapor and solid-liquid interfaces (Adamson, 1990; Bachmann et al., 2000). Drops of column buffer (10 μl) were pipetted onto the substrate; for drop sizes of 10 μl or less, gravity effects were not considered significant (Bachmann et al., 2000). Top and side view images were captured within 1 min using a desktop video camera. Sessile drop contact angles (θ_{appS}) were determined from side-view images using Eq. 2 (Colwell et al., 2003) where H is the drop height and D the length of the section in contact with the surface.

$$\theta_{app} = \left(\tan^{-1}(2H/D)\right) \times 2. \quad (2)$$

Advancing (θ_{appA}) and receding (θ_{appR}) contact angle measurements were performed using a modification of the sessile drop technique (Colwell et al., 2003). Incremental drops of column buffer (5-μl and 10-μl volumes for mica-PLL and glass, respectively) were pipetted onto the substrate. Images horizontal to the surface were captured at each increment. Receding contact angles were measured by the removal of 5- or 10-μl volumes of column buffer. All contact angle measurements were carried out at ambient laboratory relative humidity (30% ± 5%), in triplicate.

Drop spreading experiments were conducted on mica, mica-PLL, and glass substrates in triplicate. Drops of column buffer (5 μl) were pipetted onto the substrate, and the contact area of the spreading drop determined by the capture of 640 × 480 pixel movies at a frame rate of 3.75 frames s^{-1} over a 2-min time period. Drop radii were calculated from drop areas measured using ImageJ.

The influence of substrate on microfibril morphology

Adult bovine ciliary zonule or foetal bovine nuchal ligament microfibrils were adsorbed onto mica, mica-PLL, or glass substrates. Air-dried microfibrils were examined by AFM at multiple positions on each substrate. Consecutive bead/interbead repeats lying on clean substrates were extracted and straightened from 1 μm × 1 μm height scans. Individual repeats within the periodicity range 54.7–58.6 nm (29 pixels ± 1 pixel at a pixel size of 1.95 nm) were extracted and averaged.

To test the hypothesis that observed variations in microfibril morphology were substrate induced and not due to adhesion of morphologically distinct subpopulations, microfibril morphology was determined across a mica to mica-PLL interface by AFM. Gross displacements of the tip over the substrate were calculated from images captured from the Nanoscope optical viewing system calibrated against images of electron microscope grids (Athene old 400, 45 μm × 45 μm grid squares). AFM height images (3 μm × 3 μm) were captured at 12.15-μm intervals over a radial distance of 1100 μm starting at a radial position 50 μm $< r_0$ (drop radius at 0 s) and ending at a radial position 50 μm $> r_{120}$ (drop radius at 120 s). Gold particles were counted after thresholding in ImageJ. For height images with a relatively low number of adsorbed gold particles, mean RMS roughness values were calculated for three randomly placed areas (500 nm × 500 nm) within each scan. The interface between the mica and mica-PLL coated substrate was detected by an increase in surface Z-range (RMS) and the number of adhered negatively charged colloidal gold particles. Once the interface was located four (1 μm × 1 μm) AFM height scans were captured at 80-μm intervals spanning the interface region.

Hydropathy analysis

Mean hydropathy scores were calculated for amino acid sequences using the amino acid hydropathy values of Kyte and Doolittle (1982). Hydropathy profiles were calculated with a window size of 31 residues for the coding sequence following posttranslational modifications.

RESULTS AND DISCUSSION

Substrate characterization

Freshly cleaved mica imaged by AFM was featureless and atomically flat (Fig. 1 *a* (*ii* and *iii*)). Positively charged PLL in aqueous solution bound readily to the negatively charged mica following a 1-min incubation, forming aggregates of a uniform height (0.5–0.7 nm) and a vermiculate appearance (Fig. 1 *b* (*ii* and *iii*)). Surface area coverage and RMS remained constant at 39% and 0.16 nm (SD = 0.05 nm) for incubation times of up to 30 min. These observations suggest that PLL in solution forms a stable equilibrium with adsorbed PLL. Borosilicate glass coverslips exhibited longer range roughness and a ''patchy'' appearance (Fig. 1 *c* (*ii* and *iii*)). RMS roughness varied with measurement area for mica-PLL and glass substrates, but was invariant with measurement area for mica (Fig. 1 *d*). Within the linear dimensions defined by fibrillin and type-VI collagen microfibril periodicities (56–109 nm) RMS roughness varied between 0.22 and 0.23 nm (mica-PLL) and between 0.17 and 0.18 nm (glass).

The hydrophobicity/hydrophilicity of mica and mica-PLL substrates was determined macroscopically. Drop spreading on mica-PLL and glass substrates was very limited over a 2-min time course (Fig. 1 *e*). Radial displacement on mica and mica-PLL substrates attained asymptotic values <10 s after the initial contact. Spreading on mica was initially rapid followed by a gradual increase in radius over 2 min (Fig. 1 *e*). Measured column buffer sessile drop contact angles indicated that mica was hydrophilic (θ_{appS} = 21.2°, SD = 2.5°), mica-PLL less hydrophilic (θ_{appS} = 43.2°, SD = 6.0°), and glass hydrophobic (θ_{appS} = 90.3°, SD = 3.1°) at a relative humidity of 30% (Fig. 1, *a–c* (*i*)). Marked contact angle hysteresis was observed on mica-PLL substrates (Fig. 1 *f*). Contact angle hysteresis was less evident on the glass substrate (Fig. 1 *g*) and the hysteresis loop was closed.

The angle formed between the liquid-solid and liquid-vapor interfaces is called the wetting or contact angle (θ). Surfaces are defined as hydrophilic, or wettable, if $\theta < 90°$; hydrophobic, or nonwettable, if $\theta \geq 90°$, and perfectly

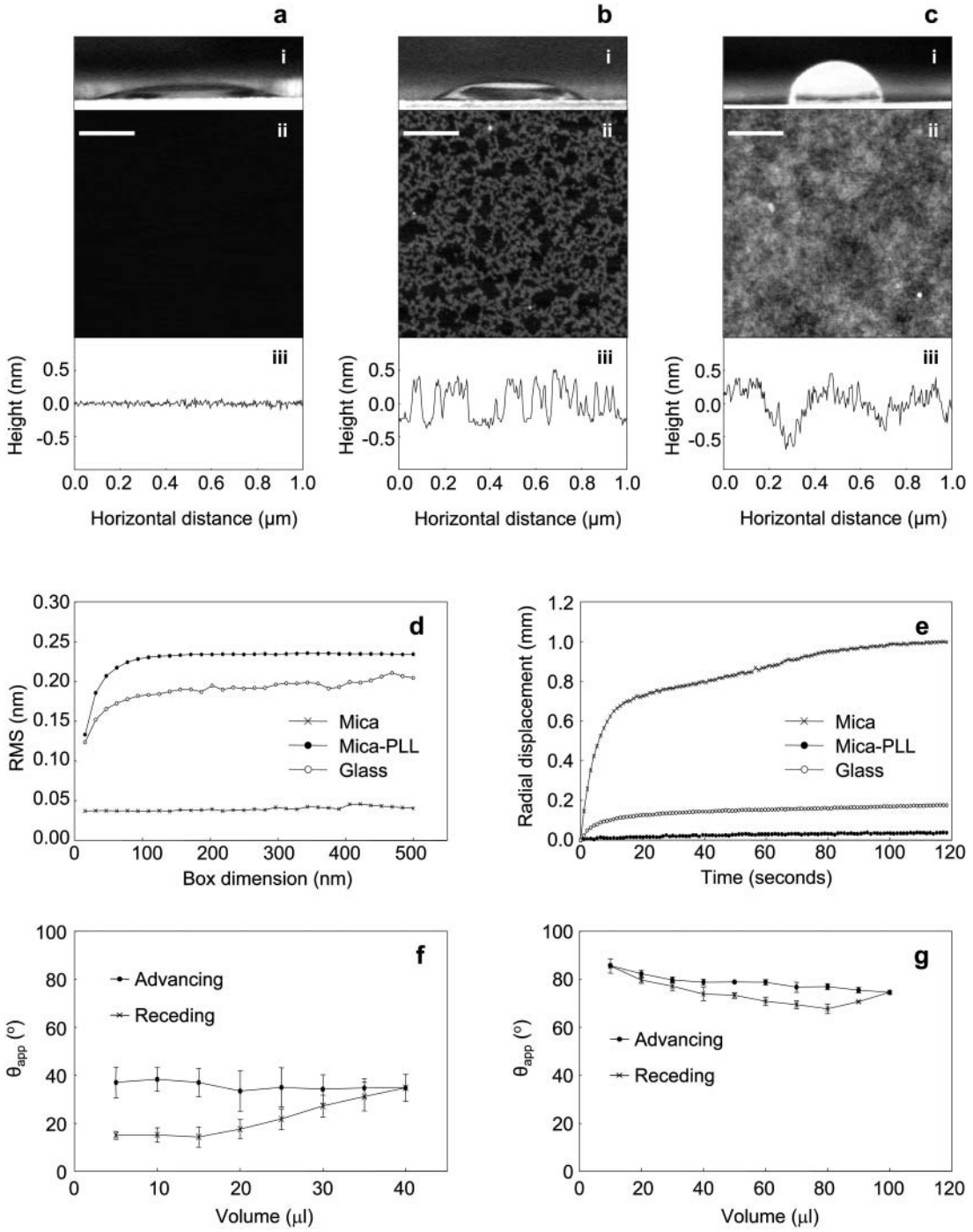

FIGURE 1 Substrate characterization. Mica, mica-PLL, and glass substrates; panels *a*, *b*, and *c*, respectively. (*i*) Side views of 10-μl column buffer drops. Substrate hydrophilicity (determined from the sessile drop contact angle θ_{appS}) decreased in the order mica (*a*), mica-PLL (*b*), and glass (*c*). (*ii*) Extracted 1 μm $\times$ 1 μm regions of 2 μm $\times$ 2 μm AFM height images, scaled to 2 nm in the *Z* direction. Freshly cleaved mica (*a*) was atomically flat. In contrast, PLL bound rapidly to mica (*b*) to form vermiculate structures 0.5–0.7-nm high. The glass substrate (*c*) presented a surface with height variations over a larger horizontal scale. (*iii*) Height profiles (1 μm) through AFM height images of mica, mica-PLL, and glass. (*d*) RMS roughness determined for box dimensions in the range 31.25–500 nm. At box dimensions of 500 nm RMS was 0.04 nm (mica), 0.23 nm (mica-PLL), and 0.20 nm (glass). (*e*) Spreading of a 5-μl drop on mica, mica-PLL, and glass substrates. Radial displacement normalized against radius at $t = 0$ s. (*f* and *g*) Advancing and receding contact angle measurements for mica-PLL (*f*) and glass (*g*) substrates. Scale bar = 200 nm.

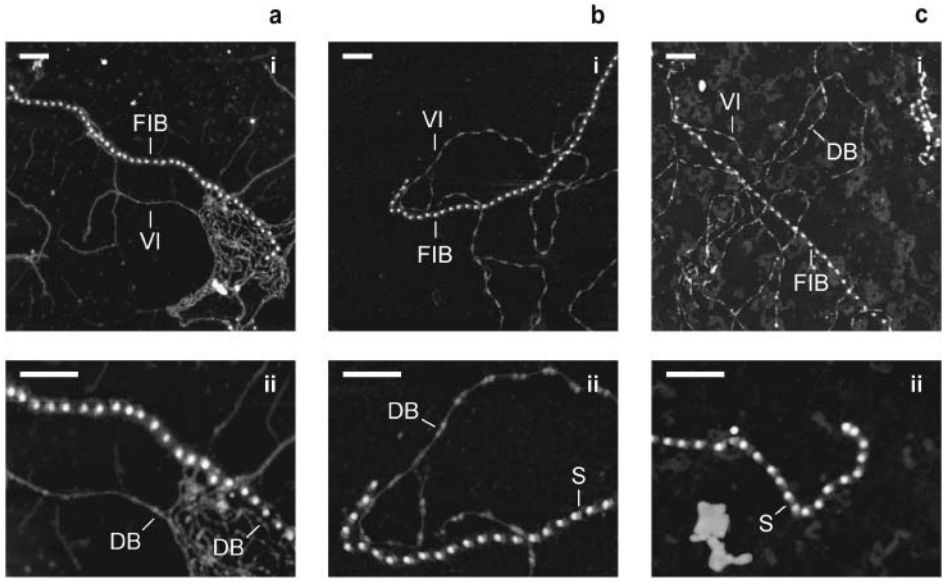

FIGURE 2 Substrate-dependent morphology of copurified fibrillin and type-VI collagen microfibrils. (*a–c*) AFM height images of foetal bovine nuchal ligament microfibrils adsorbed on mica (*a*), mica-PLL (*b*), and glass (*c*) substrates; panels *a–c* (*i*) 2 μm $\times$ 2 μm; panels *a–c* (*ii*) 1 μm $\times$ 0.75 μm. Fibrillin microfibrils (*FIB*) and type-VI collagen microfibrils (*VI*) extracted from the same tissue sample were identified on all substrates. Fibrillin microfibrils on mica (*a*) appeared diffuse with no shoulder regions adjacent to the beads. On mica-PLL and glass substrates (*b* and *c*), fibrillin microfibrils were more closely packed with a pronounced shoulder region (*S*) adjacent to the bead. The characteristic double bead (*DB*) of type-VI collagen microfibrils was preserved on mica-PLL and glass (*b* and *c*) but on the more hydrophilic mica double-beaded regions were only identifiable within, or at the periphery of, microfibrillar bundles. The characteristic morphology and periodicity of type-VI collagen microfibrils was largely absent on the mica surface. *Z* scale = 8 nm. Scale bar = 200 nm.

wettable if θ is zero or nonmeasureable (Dury et al., 1998; Sweeney et al., 1993). On perfectly wettable surfaces, drops of water spread completely (Sweeney et al. 1993), on partially wettable (hydrophilic) or nonwettable (hydrophobic) surfaces, drops of liquid assume a shape, which depends on the relation between the free energies of the three involved surfaces. Experimentally, on nonideal surfaces, the measured contact angle (apparent contact angle; θ_{app}) will be an average of microscopic contact angles (θ_m) that follow local surface deformations (Dury et al., 1998). Although measurements are commonly made on a sessile drop (Bachmann et al., 2000), on most solid surfaces the measured contact angle as the drop advances (θ_{appA}) across the surface is different from contact angle measured as the drop recedes (θ_{appR}). This difference in advancing and receding contact angles, denoted as contact angle hysteresis (Schwartz and Garoff, 1985), may be induced by surface roughness or chemical heterogeneities (de Gennes, 1985).

Cleaving mica forms an atomically smooth chemically homogeneous substrate that would not be expected to exhibit contact angle hysteresis. The apparent contact angle of 21.2° indicates that the mica substrate was relatively wettable/hydrophilic. Glass substrates had advancing contact angles (θ_{appA}) that decreased from 85° to 74° with increasing drop volume (Fig. 1 *g*), an effect that may be due to gravity (Bachmann et al., 2000). The relatively small contact angle hysteresis may be due to surface roughness, although some studies suggest that the effects of surface roughness on contact angle hysteresis are minimal when roughness is $<$100 nm (Neumann and Good, 1972; Extrand and Kumagai, 1997) and that surface chemistry is more important (Extrand and Kumagai, 1997). Glass and mica-PLL substrates are of comparable roughness but mica-PLL substrates exhibit large contact angle hysteresis effects (Fig. 1, *f* and *g*). We would suggest therefore, that roughness at the sub-nm scale does not explain the differences observed in hysteresis in these two systems. In general the contact angle of clean glass surfaces and water is close to 0° with glass hydrophobicity a consequence of the adsorption of organic substances from the atmosphere (Takeda et al., 1999). The mica-PLL system is chemically heterogeneous, and it is likely that the glass substrate is also chemically heterogeneous; therefore the differences in hysteretic behavior may be attributable to the extent and chemical nature of the heterogeneity. Kinetic hysteresis may dominate on mica-PLL substrates as the adsorbed PLL molecules swell or reorganize in the liquid phase (Morra et al., 1990). The spreading behavior and apparent sessile drop contact angles suggest that each of the three substrates is partially wettable in the system substrate-sodium chloride solution air, although the degree of wettability decreases in the order mica $>$ mica-PLL $>$ glass.

Mica minerals are layered crystals in which tetrahedral sheets of $(Si, Al)_2O_5$ are ionically linked by a central $Al_2(OH)_2$ layer (Bailey, 1984). In the uncleaved muscovite mica crystal the net negative charge of basal oxygens is balanced by a layer of hexagonally coordinated K^+ cations. Following cleavage, this layer is completely neutralized by the negative aluminosilicate lattice (Gaines and Tabor, 1956). In water some of the K^+ ions dissociate from the surface resulting in a negative surface charge density of 15,000 negative charges/μm^2 at neutral pH (Pashley, 1981;

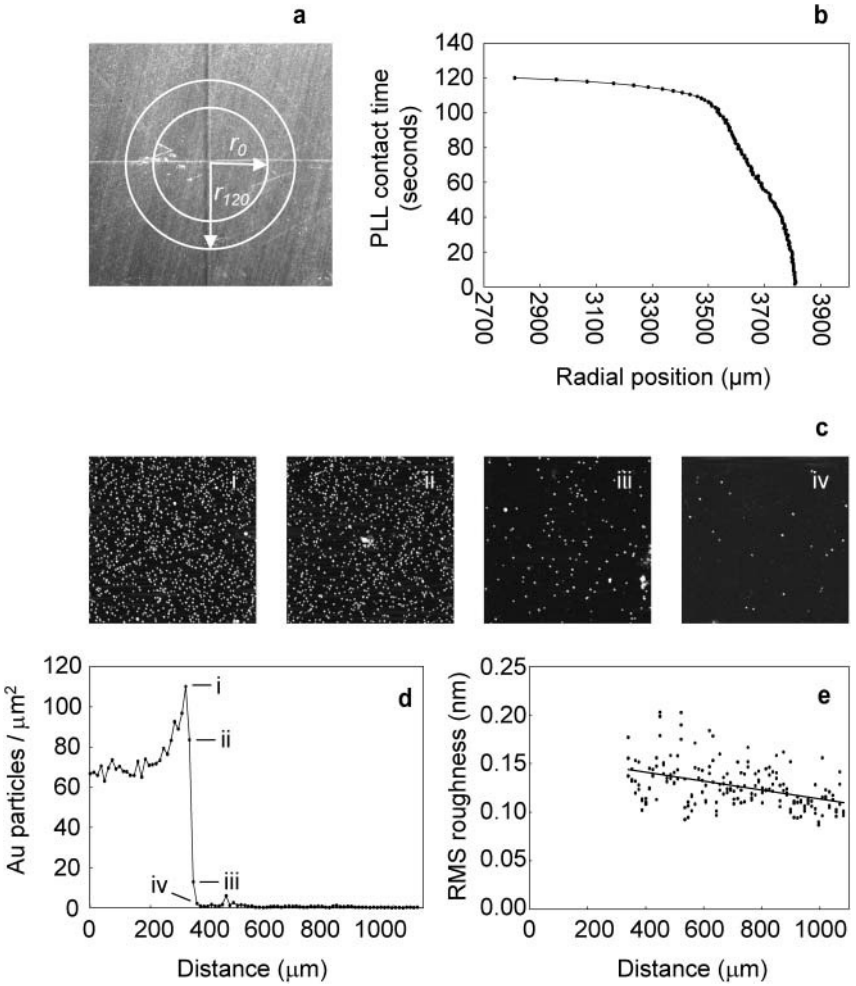

FIGURE 3 Mica to mica-PLL gradient characterization. (*a*) Top view mica adhered to metal support stub scored with radial lines. Liquid drops (5 μl) spread from radial position r_0 to r_{120} during 2-min incubations. (*b*) Calculated PLL contact time as a function of radial position. (*c*) AFM height images (3 μm $\times$ 3 μm) captured at 12.15-μm intervals spanning the gold particle interface. (*d*) Profile of gold particle adsorption over a 1100-μm radial distance. The radial positions of scans *i–iv* in panel *c* are marked. (*e*) RMS substrate roughness measured from point *iv* (350 mm) on panel *d*. The data points fit a linear regression with an r^2 value of 0.2. *Z* scale = 10 nm.

Muller et al., 1997) presenting a hydrophilic surface (Kowalewski and Holtzman, 1999). Subsequent microfibril adsorption experiments were carried out in a salt solution. Microfibril preparations were eluted from the size exclusion column in a 400 mM NaCl solution buffered to a pH of 7.4 by 50 mM Tris-HCl and 10 mM $CaCl_2$ was present in the collagenase digestion buffer. In salt solutions, the extent of the dissociated and replaced K^+ ions from the mica surface depends on the electrolyte concentration (Gaines and Tabor, 1956; Pashley, 1981). The surface charge in solution is balanced by bound counterions that form the Helmholtz layer and a diffuse charge cloud, the electric double layer (Muller et al., 1997). Cations bind to the negatively charged surface rendering the mica positively charged (Forbes et al., 2001). Therefore, during adsorption of microfibrils to mica the surface was hydrophilic and positively charged. Previous studies have demonstrated that adsorbed PLL reverses the negative charge of mica and silica (Luckham and Klein, 1984; Velegol and Tilton, 2001). The adsorption of negatively charged colloidal gold in the absence of divalent cations also suggests that PLL reverses the charge of mica. The influence of Helmholtz and electric double layers would be reduced on a positively charged surface. The low wettability of glass coverslips may be due to adsorption of atmospheric substances by surface OH groups (Takeda et al., 1999). From our data we conclude that microfibrils adsorbing to glass will encounter a hydrophobic microenvironment and mica-PLL will present a less hydrophilic microenvironment than mica alone.

Substrate-dependent morphology of fibrillin microfibrils

Fibrillin microfibrils isolated from foetal bovine nuchal ligament were identified by their unique repeating beaded structure and untensioned periodicity of ~56 nm on mica, mica-PLL, and glass substrates, (Fig. 2, *a–c*) (Sherratt et al., 2001). Fibrillin microfibrils adsorbed on the hydrophilic mica substrate had a diffuse appearance (Fig. 2 *a*). Microfibrils adsorbed to the less hydrophilic mica-PLL substrate appeared more condensed with a shoulder region (bead asymmetry), which conferred an orientation to the microfibril (Fig. 2 *b*). Morphologically indistinguishable microfibrils were observed on glass substrates (Fig. 2 *c*). Similar variations in microfibril morphology have been reported for microfibrils visualized by rotary shadowing transmission

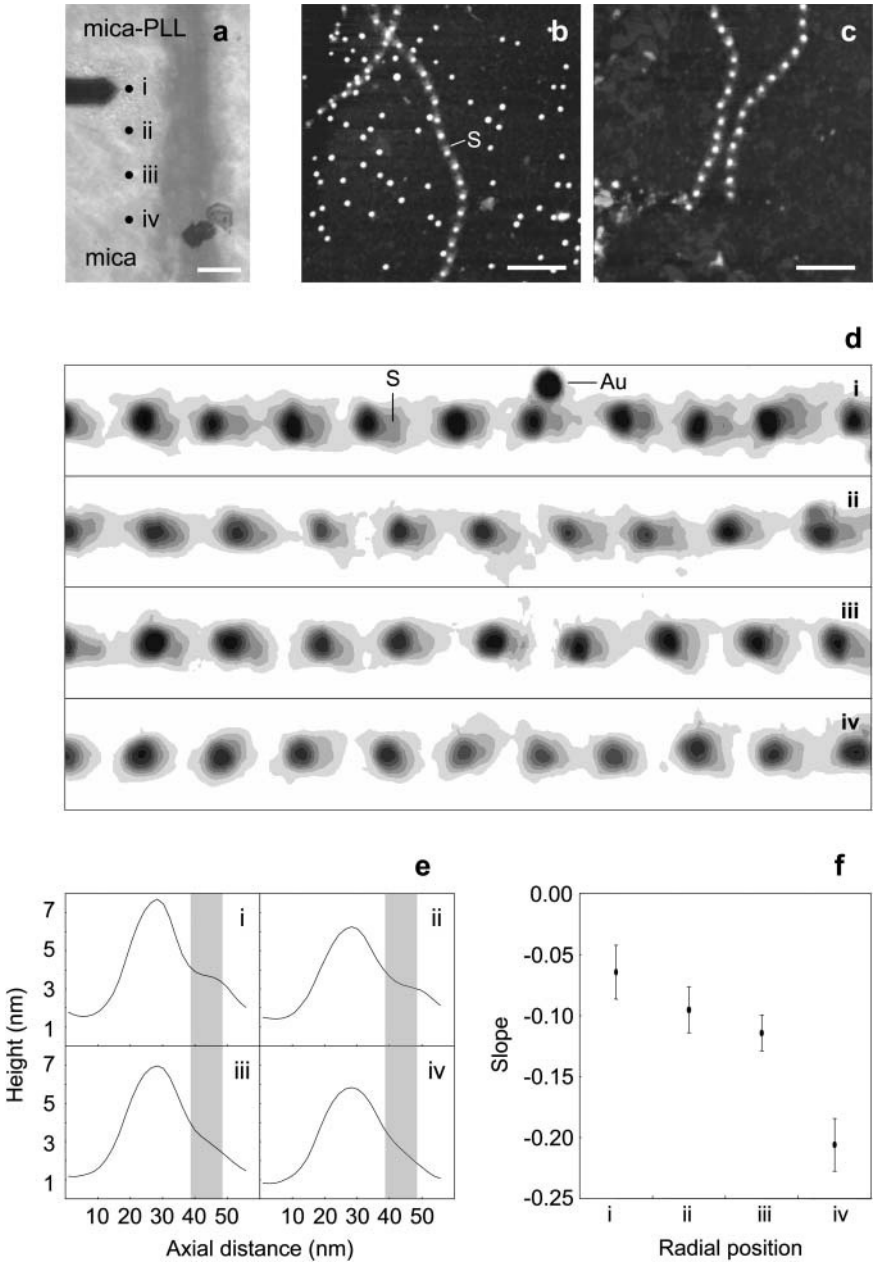

FIGURE 4 Substrate-dependent fibrillin microfibril morphology. (*a*) Optical micrograph of the AFM cantilever, substrate, and four positions (*i–iv*) spanning the mica-PLL (*i*) to mica (*iv*) interface. Sequential AFM height images of adult bovine ciliary zonule microfibrils (1 μm $\times$ 1 μm) were captured at 80-μm intervals along a radius from the edge of the gold adsorption zone to a radial position of +240 μm. (*b*) 1 μm $\times$ 1 μm AFM height image captured at position *i*. Many negatively charged colloidal gold particles were bound to the positively charged PLL. Fibrillin microfibrils were closely packed with an oriented shoulder region (*S*). (*c*) 1 μm $\times$ 1 μm AFM height image captured at position *iv*. The substrate was devoid of adsorbed colloidal gold particles; microfibril morphology was diffuse with no oriented shoulder regions adjacent to the beads. (*d*) Height contour maps of straightened microfibril sections (600 nm $\times$ 80 nm extracted regions from 1 μm $\times$ 1 μm scans) from AFM scans at positions *i–iv*. As PLL concentration decreased from *i* to *iv*, fibrillin microfibrils were more diffuse in appearance, shoulder regions (*S*) were progressively lost, and colloidal gold particles (*Au*) were absent. (*e*) Mean central axial height distributions (width = 1.95 nm) calculated from the consecutive repeats in *d*. Shoulder regions (denoted by *shaded bars*) were well defined on mica-PLL (*i*), less well defined at radial positions of +80 μm and +160 μm (*ii* and *iii*), and absent at a radial position of +240 μm. (*f*) The slope within the shoulder region became more pronounced from radial positions *i–iv*.

electron microscopy (TEM) (Wright and Mayne, 1988; Kielty et al., 1991). Although the removal of aqueous solvent during air drying may affect microfibril morphology, recent studies have demonstrated that the major structural features identified by electron microscopy and AFM in dehydrated microfibrils such as the bead/interbead structure, periodicity, and shoulder region are also present in fully hydrated microfibrils in solution (Sherratt et al., 2003). We suggest that the charge on mica has a profound effect on microfibril morphology and that mica-PLL and glass substrates induce fewer morphological rearrangements on adsorption.

Although members of the fibrillin family of proteins are the major constituents of fibrillin microfibrils, it is likely that microfibrils are heteropolymers, the composition of which may vary both within and between tissues (Kielty et al., 2002b). Given the reported variability of microfibril composition, the diffuse and condensed morphologies observed on mica and mica-PLL/glass substrates, respectively, could result from the substrate-specific adsorption of compositionally and hence morphologically distinct subpopulations. To test this hypothesis, microfibrils were adsorbed onto a mica substrate with a central PLL-coated region. The PLL drop spread over the mica surface during the 2-min incubation period (Fig. 3, *a* and *b*). Drop spreading provides a mechanism for the creation of a PLL gradient. At the radial position r_0 the mica substrate as exposed to PLL for 2 min, between radial positions of 3500–3807 μm there was an approximately linear decrease in mica to PLL contact time (Fig. 3 *b*). Gold particles

required a critical amount of adsorbed PLL to adhere to the substrate (Fig. 3 *d*), but the amount of adsorbed PLL decreased in a linear fashion after this point as determined by RMS roughness measurements (Fig. 3 *e*). The position of the mica-PLL/mica interface was located by the adsorption/nonadsorption of 10-nm diameter negatively charged colloidal gold spheres that only bound to the positively charged PLL (Fig. 4 *b*). If the observed morphologies were substrate induced then microfibrils with an intermediate morphology would be observed at the interface. At positions flanking the interface, fibrillin microfibril morphologies were similar to those observed previously, diffuse on mica (Fig. 4 *d* (*iv*)) and condensed with a pronounced shoulder region on mica-PLL (Fig. 4 *d* (*i*)). Fibrillin microfibrils at positions *ii* and *iii*, which lie within the mica to mica-PLL interface (Fig. 4 *d* (*ii* and *iii*)), had an intermediate morphology with a shoulder region that was more pronounced than on mica (Fig. 4 *e* (*i*)) but less pronounced than on mica-PLL (Fig. 4 *e* (*iv*)). The calculated axial slope within this plateau region increased between positions *i–iv* (Fig. 4 *f*). We conclude that distinct microfibrillar morphologies are substrate induced rather than substrate selected.

The morphology of adsorbed fibrillin microfibrils may be influenced by the hydrophobicity/hydrophilicity of both the substrate and the microfibrils. Hydropathy profiles repetitively average numerical values (the hydropathy index) assigned to each amino acid in a protein sequence. The Kyte and Doolittle hydropathy profile of human fibrillin-1 is slightly hydrophilic (Swiss-Prot P3555; hydropathy score = −0.434) (Fig. 5 *a*). The protein becomes gradually more hydrophilic in the N- to C-terminus direction and the N- and C-termini are both highly hydrophilic. Human fibronectin is an ECM protein with a similar hydropathy score (Swiss-Prot P02751; hydropathy score = −0.554) and an overall structure, which is stabilized by ionic interactions between negative and positive domains. AFM studies of fibronectin identified an extended morphology on hydrophilic and a condensed morphology on hydrophobic substrates (Bergkvist et al., 2003). Hydrophilic substrates may disrupt interdomain ionic interactions inducing an extended fibronectin morphology and a diffuse fibrillin microfibril morphology. Sample-substrate interactions on hydrophobic substrates are thought to be dominated by relatively weak van der Waals forces and hydrogen bonds (Betley et al., 2001). These weak interactions may not interfere with intermolecular ionic interactions reducing substrate-induced distortion of the sample. As with fibronectin (Bergkvist et al., 2003) and synthetic dendrimers (Betley et al., 2001) the morphology of fibrillin microfibrils on mica-PLL and glass may more closely resemble the morphology in solution than fibrillin microfibrils adsorbed to mica.

Bead shoulder regions have been identified in microfibrils imaged by scanning TEM, AFM, and automated electron tomography (Sherratt et al., 1997; Hanssen et al., 1998; Baldock et al., 2001). The disruption of the shoulder region on mica substrates identifies an axially located region of the microfibril, which is particularly sensitive to local charge environments. Although the amino acid sequence of fibrillin-1 is predominantly hydrophilic (Fig. 5 *b*), there are no extended regions of increased hydrophilicity. Fibrillin-1 is a glycoprotein with 12 potential *N*-glycosylation sites. N-linked glycosylation of recombinant putative glycosylation sites within fibrillin-1 peptides has been demonstrated by shifts in electrophoretic mobility following endoglycosidase H treatment (Ashworth et al., 1999). Complex N-linked oligosaccharides are negatively charged if they contain sialic

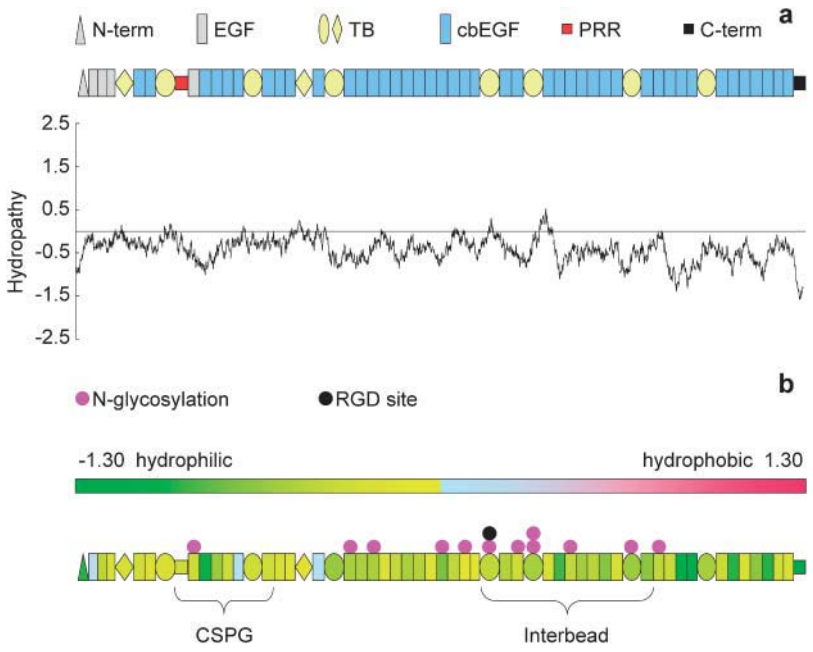

FIGURE 5 Fibrillin-1 hydropathy profile and folding model. (*a*) Kyte and Doolittle hydropathy profile and domain map of human fibrillin-1. (*b*) Domain hydropathy map. Individual domain hydropathies are color coded on a scale of from −1.30 (hydrophilic) to 1.30 (hydrophobic). Putative glycosylation sites are marked in pink, the potential cell attachment site (*RGD*) is marked in black. Regions of the monomer thought to lie within the interbead and to which CSPGs bind are marked by braces.

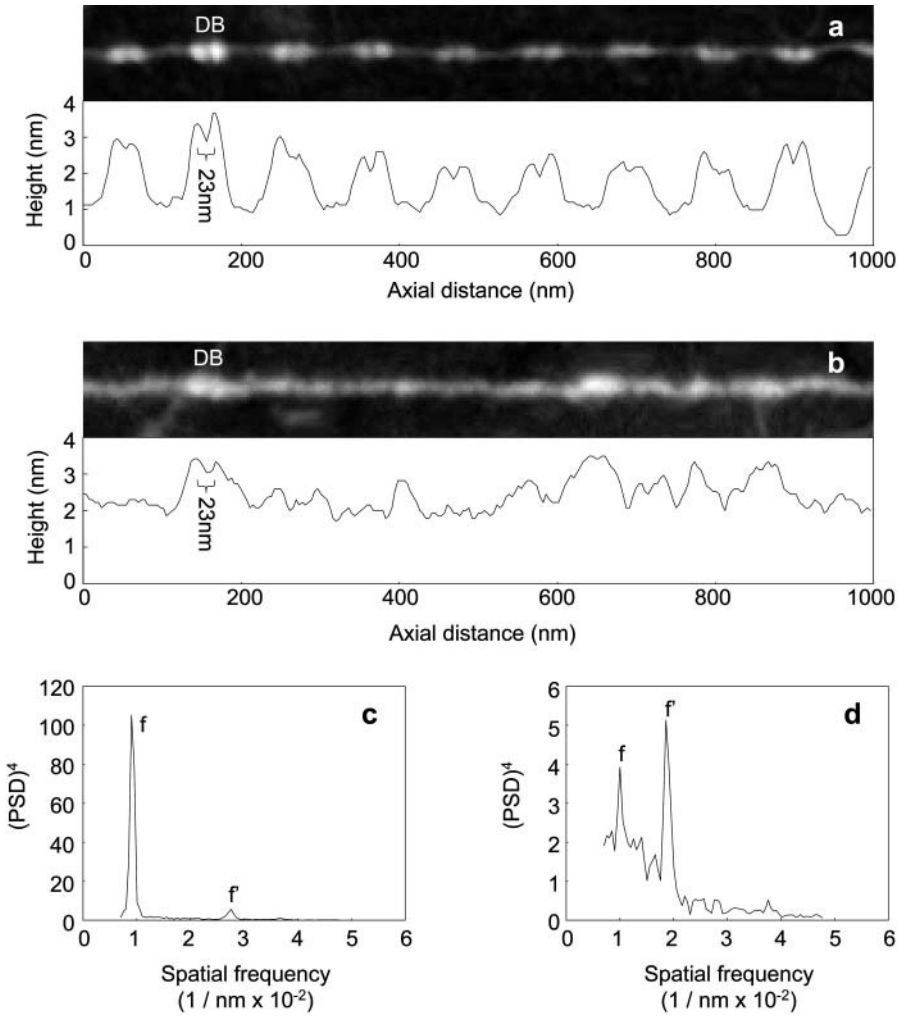

FIGURE 6 Type-VI collagen morphology and periodicity. (*a*) Straightened AFM height image (1000 × 120 nm) and axial height distribution of a type-VI collagen microfibril on mica-PLL. Primarily noncollagenous double beads (*DB*) spaced 108.3 nm apart (SD = 7.8 nm) are separated by tetramers of triple helical collagen with a height of ~1 nm. (*b*) Straightened AFM height image and axial height distribution for a type-VI collagen microfibril from the same preparation adsorbed to a mica substrate. Double beads (*DB*) were occasionally identifiable by height (>3 nm) and bead-to-bead distance (~23 nm). (*c* and *d*) Power spectral density analyses of type-VI collagen microfibril periodicity on mica-PLL (*c*) and mica (*d*) substrates. Within type-VI collagen microfibrils on mica-PLL the fundamental frequency (*f*) was within the range 100–117 nm (peaking at 110 nm); a third-order harmonic (*f*′) was also identified at 36 nm. On the mica substrate the fundamental frequency (*f*) was within the range 96–105 nm (peaking at 100 nm); a strong second-order harmonic (*f*′) peaked at 54 nm. Height image *Z* scale = 4 nm.

acid. Many of the glycosylation sites are within a section of the monomer, which is predicated to lie within the interbead region within the microfibril (Baldock et al., 2001). Interactions between hydrophilic N-linked oligosaccharides and the hydrophilic mica may cause structural rearrangements that disrupt the shoulder region. Additional regions of increased hydrophilicity may result form the heteropolymeric nature of fibrillin microfibrils. TEM and scanning TEM ultrastructural approaches including cuprolinic blue staining (Kielty et al., 1996) and mass changes following enzymatic digestion (Sherratt et al., 1997) provided strong evidence for an association of chondroitin sulfate proteoglycans (CSPGs) with the fibrillin microfibril bead. A small sulphated CSPG interacts with fibrillin-1 at a site within or adjacent to the proline-rich region (Trask et al., 2000). CSPGs consist of a core protein and one or more highly negatively charged glycosaminoglycan (GAG) side chains. The structure of a shoulder region composed of associated CSPG and hydrophilic GAGs may be disrupted by a hydrophilic substrate. Substrate-dependent interactions have been demonstrated between fibrillin-1 fragments and microfibril associated molecules, tropoelastin, and MAGP-1 (Rock et al., 2004).

Isolated microfibrils have been shown to support the attachment of vascular smooth muscle cells (Kielty et al., 1992) and cell-specific integrins $\alpha_5\beta_1$ and $\alpha_v\beta_3$ induce cell spreading, alter cytoskeletal organization, and upregulate fibrillin-1 synthesis (Bax et al., 2003). Substrate-induced conformational changes may alter cellular recognition of fibrillin microfibrils by RGD (Arg-Gly-Asp) site masking or by relative movement of the RGD and potential synergy sites (Krammer et al., 2002). The RGD site is located within the interbead region in close proximity to a number of N-linked glycosylation sites (Fig. 5 *b*). Microfibril-associated molecules such as MAGP-1, tropoelastin, and fibulin-2 are thought to bind at or near the proline-rich region (Rock et al., 2004). Substrate-induced changes in GAG conformation may mediate the binding of associated molecules. Local charge environments may also affect fibrillin microfibril morphology in vivo. The vertebrate elastic fiber is composed of fibrillin microfibrils and highly hydrophobic elastin (Swiss-Prot P15502; hydropathy score = 0.706). It is not

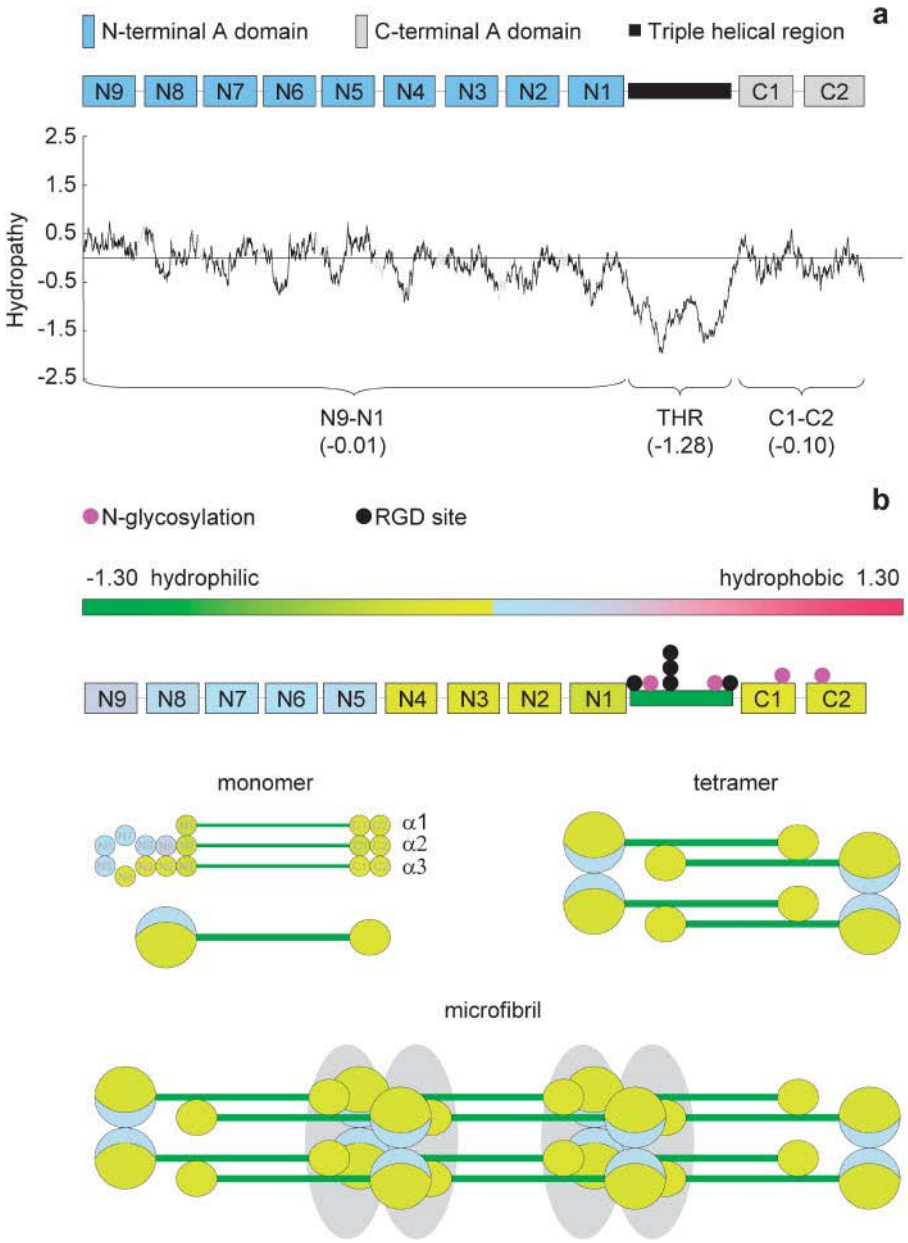

FIGURE 7 Type-VI collagen hydropathy profile, and domain/microfibril hydropathy map. (*a*) Kyte and Doolittle hydropathy profile and domain map of human α_3(VI); vWFA domains (*blue* or *gray*), triple helical region (*black*), unique regions (*shaded line*). Mean vWFA hydropathy scores indicate that vWFA domains are neither hydrophobic or hydrophilic. The triple helical region is highly hydrophilic. (*b*) Mean domain hydropathies mapped onto the current model of type-VI collagen assembly (Furthmayr et al., 1983; Baldock et al., 2003) Putative glycosylation sites are marked in pink; potential cell attachment sites (*RGD*) are marked in black. Within the N-terminal globular region hydrophobic domains are confined to one side of the loop formed by α_3(N2–N9); the remainder of the vWFA domains in the N- and C-terminal globular regions are slightly hydrophilic. These domains may form a stabilizing hydrophobic pocket within each double bead in the assembled microfibril.

clear whether elastin-associated microfibrils differ morphologically and functionally from those that do not associate with elastin (Kielty et al., 2002a). We suggest that local charge environment conformational changes may also occur in vivo acting as a molecular switch to hide or reveal binding sites in compositionally identical elastin-associated and nonelastin-associated fibrillin microfibrils.

Substrate-dependent morphology of type-VI collagen microfibrils

Type-VI collagen microfibrils have a unique and complex repeating double-bead structure with an untensioned periodicity of 104–112 nm (Ball et al., 1999; Baldock et al., 2003). Beads are composed primarily of the noncollagenous N- and C-terminal regions and the interbead of four collagen triple helical regions (Furthmayr et al., 1983; Baldock et al., 2003). Type-VI collagen microfibrils isolated from foetal bovine nuchal ligament had well-defined double-bead and interbead regions when adsorbed to a mica-PLL substrate (Fig. 2 *b*). As with fibrillin microfibrils, morphologically indistinguishable assemblies were observed on mica-PLL and glass substrates (Fig. 2 *c*). Beads had a maximum height of ~3 nm and interbeads were ~1 nm in height (Fig. 6 *a*). Type-VI collagen microfibrils, isolated from foetal bovine nuchal ligament and aorta, with similar bead/interbead heights and repeating periodicities have previously been identified on PLL-coated mica substrates by AFM (Baldock

et al., 2003). Adsorption to a mica substrate induced major morphological changes (Figs. 2 *a* and 6 *b*). The characteristic double-bead/interbead structure was largely absent and periodicity could not be determined visually (Fig. 6 *b*). These structures were identified as type-VI collagen microfibrils using a number of observations. In regions of the mica surface where these structures formed bundles, double beads were clearly identifiable (Fig. 2 *a* (*ii*)). Double beads with a similar height maximum to mica-PLL double beads were occasionally observed on regions of the microfibril exposed to bare mica (Fig. 6 *b*). Power spectral density analyses of these structures revealed an underlying periodicity very similar to the reported periodicity of type-VI collagen microfibrils and the periodicity measured on mica-PLL (Figs. 6, *c* and *d*). Unlike the region-specific conformational changes observed for fibrillin microfibrils, type-VI collagen microfibrils respond to more hydrophilic environments with major structural rearrangements along the whole repeating unit.

The noncollagenous domains of type-VI collagen have a mean hydropathy very close to zero (Fig. 7 *a*) (Swiss-Prot P12111 α_3(VI) N9–N1 = −0.01). The triple helical region is highly hydrophilic and the RGD sites are clustered in this region. Color-coding domains according to mean hydropathy revealed that most of the noncollagenous domains are slightly hydrophilic (α_3(VI) N1–N4 mean = −0.198) but α_3(VI) domains (N5–N9) are slightly hydrophobic (mean = 0.139). The current folding model of the type-VI collagen N-terminal globular region predicts that these domains will form a loop located on one side of the N-terminal globular region (Specks et al., 1992; Baldock et al., 2003). In the assembled microfibril, these hydrophobic faces may come into contact forming a hydrophobic pocket, which helps to stabilize the microfibril. It is unlikely that these hydrophobic interactions play a role in microfibril assembly as α_3(VI) N5–N9 domains are not needed for microfibril assembly (Lamande et al., 2002). We propose that the difference in morphology is due to the higher exposure of charged groups on the microfibril to the charged hydrophilic mica. In contrast to the localized charge within fibrillin microfibrils, the highly charged triple helical region of type-VI collagen spans the whole repeat (Baldock et al., 2003). The majority of the globular domains in type-VI collagen have homology to von Willebrand factor (vWF) A domains and vWF itself has been shown to be sensitive to the local surface charge environment. On a modified hydrophobic glass surface, adsorbed vWF appeared compact by AFM, on a hydrophilic mica surface, vWF extended to cover a greater surface area (Raghavachari et al., 2000).

CONCLUSIONS

Substrate-dependent conformations have previously been observed for isolated proteins. Our data demonstrates that the local surface environment may also induce profound changes in the morphology of large isolated supramolecular assemblies. Fibrillin microfibrils and type-VI collagen microfibrils are biochemically distinct assemblies. Therefore substrate-induced conformational rearrangements may occur in most adsorbed protein structures.

The increasing reliance on solid-phase binding assays to investigate protein-protein and protein-cell interactions highlights the importance of physisorption effects on protein function. Local charge environments may also induce conformational changes in supramolecular assemblies in vivo. Elastin-associated fibrillin microfibrils may differ from nonelastin-associated microfibrils only in their charge environment induced conformation and not in composition.

The authors thank Miss Amanda Morgan for expert technical assistance.

M.J.S. and C.M.K. acknowledge the support of the Medical Research Council (UK). D.F.H. acknowledges the support of the Wellcome Trust.

REFERENCES

Adamson, A. W. 1990. Physical Chemistry of Surfaces. John Wiley and Sons, New York.

Ashworth, J. L., G. Murphy, M. J. Rock, M. J. Sherratt, S. D. Shapiro, C. A. Shuttleworth, and C. M. Kielty. 1999. Fibrillin degradation by matrix metalloproteinases: implications for connective tissue remodelling. *Biochem. J.* 340:171–181.

Bachmann, J., A. Ellies, and K. H. Hartge. 2000. Development and application of a new sessile drop contact angle method to assess soil water repellency. *J. Hydrol.* 231–232:66–75.

Bailey, S. W. 1984. Crystal-chemistry of the true micas. *Rev. Miner.* 13: 13–60.

Baldock, C., A. J. Koster, U. Ziese, M. J. Rock, M. J. Sherratt, K. E. Kadler, C. A. Shuttleworth, and C. M. Kielty. 2001. The supramolecular organisation of fibrillin-rich microfibrils. *J. Cell Biol.* 152:1045–1056.

Baldock, C., M. J. Sherratt, C. A. Shuttleworth, and C. M. Kielty. 2003. The supramolecular organization of collagen VI microfibrils. *J. Mol. Biol.* 330:297–307.

Ball, S. G., K. Johnston, C. M. Kielty, and C. A. Shuttleworth. 1999. STEM mass mapping of type VI collagen microfibrils: implications for chain composition and alternative splicing. *Proc. Ind. Acad. Sci.* 111:147–157.

Bax, D. V., S. E. Bernard, A. Lomas, A. Morgan, J. Humphries, C. A. Shuttleworth, M. J. Humphries, and C. M. Kielty. 2003. Cell adhesion to fibrillin-1 molecules and microfibrils is mediated by $\alpha5\beta1$ and $\alpha v\beta3$ integrins. *J. Biol. Chem.* 278:34605–34616.

Bellingham, C. M., K. A. Woodhouse, P. Robson, S. J. Rothstein, and F. W. Keeley. 2001. Self-aggregation characteristics of recombinantly expressed human elastin polypeptides. *Biochim. Biophys. Acta.* 1550: 6–19.

Bergkvist, M., J. Carlsson, and S. Oscarsson. 2003. Surface-dependent conformations of human plasma fibronectin adsorbed to silica, mica, and hydrophobic surfaces, studied with use of atomic force microscopy. *J. Biomed. Mater. Res.* 64A:349–356.

Betley, T. A., M. M. Banaszak Holl, B. G. Orr, D. R. Swanson, D. A. Tomalia, and J. R. Baker. 2001. Tapping mode atomic force microscopy investigation of poly(amidoamine) dendrimers: effects of substrate and pH on dendrimer deformation. *Langmuir.* 17:2768–2773.

Colwell, J. M., E. Wentrup-Byrne, J. M. Bell, and L. S. Wielunski. 2003. A study of the chemical and physical effects of ion implantation pf microporous and nonporous PTFE. *Surf. Coat. Tech.* 168:216–222.

de Gennes, P. G. 1985. Wetting: statics and dynamics. *Rev. Mod. Phys.* 57:827–863.

Dury, O., U. Fischer, and R. Schulin. 1998. Dependence of hydraulic and pneumatic characteristics of soils on a dissolved organic compound. *J. Contam. Hydrol.* 33:39–57.

Extrand, C. W., and Y. Kumagai. 1997. An experimental study of contact angle hysteresis. *J. Colloid Interface Sci.* 191:378–383.

Forbes, J. G., A. J. Jin, and K. Wang. 2001. Atomic force microscope study of the effect of the immobilization substrate on the structure and force-extension curves of a multimeric protein. *Langmuir.* 17:3067–3075.

Furthmayr, H., H. Wiedemann, R. Timpl, E. Odermatt, and J. Engel. 1983. Electron-microscopical approach to a structural model of intima collagen. *Biochem. J.* 211:303–311.

Gaines, G. L., and D. Tabor. 1956. Surface adhesion and elastic properties of mica. *Nature.* 170:1304–1305.

Garcia, A. J., M. D. Vega, and D. Boettiger. 1999. Modulation of cell proliferation and differentiation through substrate-dependent changes in fibronectin conformation. *Mol. Biol. Cell.* 10:785–798.

Grinnell, F., and M. K. Feld. 1981. Adsorption characteristics of plasma fibronectin in relationship to biological activity. *J. Biomed. Mater. Res.* 15:363–381.

Hanssen, E., S. Franc, and R. Garrone. 1998. Atomic force microscopy and modelling of natural elastic fibrillin polymers. *Biol. Cell.* 90:223–228.

Haynes, C. A., and W. Norde. 1995. Structures and stabilities of adsorbed proteins. *J. Colloid Interface Sci.* 169:313–328.

Kielty, C. M., C. Cummings, S. P. Whittaker, C. A. Shuttleworth, and M. E. Grant. 1991. Isolation and ultrastructural analysis of microfibrillar structures from foetal bovine elastic tissues. Relative abundance and supramolecular architecture of type VI collagen assemblies and fibrillin. *J. Cell Sci.* 99:797–807.

Kielty, C. M., and M. E. Grant. 2002. The collagen family: structure, assembly and organisation in the extracellular matrix. *In* Connective Tissue and its Heritable Disorders, 2nd ed. P. M. Royce and B. Steinmann, editors. Wiley, New York. 159–221.

Kielty, C. M., M. J. Sherratt, and C. A. Shuttleworth. 2002a. Elastic fibres. *J. Cell Sci.* 115:2817–2828.

Kielty, C. M., T. J. Wess, L. Haston, J. L. Ashworth, M. J. Sherratt, and C. A. Shuttleworth. 2002b. Fibrillin-rich microfibrils: elastic biopolymers of the extracellular matrix. *J. Muscle Res. Cell Motil.* 23:581–596.

Kielty, C. M., S. P. Whittaker, M. E. Grant, and C. A. Shuttleworth. 1992. Attachment of human vascular smooth muscles cells to intact microfibrillar assemblies of collagen VI and fibrillin. *J. Cell Sci.* 103:445–451.

Kielty, C. M., S. P. Whittaker, and C. A. Shuttleworth. 1996. Fibrillin: evidence that chondroitin sulphate proteoglycans are components of microfibrils and associate with newly synthesised monomers. *FEBS Lett.* 386:169–173.

Keselowsky, B. G., D. M. Collard, and A. J. Garcia. 2003. Surface chemistry modulates fibronectin conformation and directs integrin binding and specificity to control cell adhesion. *J. Biomed. Mater. Res.* 66A:247–259.

Kocsis, E., B. L. Trus, C. J. Steer, M. E. Bisher, and A. C. Steven. 1991. Imaging averaging of flexible fibrous macromolecules: the clathrin triskeleton has an elastic proximal segment. *J. Struct. Biol.* 107:6–14.

Kowalewski, T., and D. M. Holtzman. 1999. In situ atomic force microscopy study of Alzheimer's beta-amyloid peptide on different substrates: new insights into mechanism of beta-sheet formation. *Proc. Natl. Acad. Sci. USA.* 96:3688–3693.

Krammer, A., D. Craig, W. E. Thomas, K. Schulten, and V. Vogel. 2002. A structural model for force regulated integrin binding to fibronectin's RGD-synergy site. *Matrix Biol.* 21:139–147.

Kyte, J., and R. Doolittle. 1982. A simple method for displaying the hydropathic character of a protein. *J. Mol. Biol.* 157:105–132.

Lamande, S. R., M. Morgelin, C. Selan, G. J. Jobsis, F. Baas, and J. F. Bateman. 2002. Kinked collagen VI tetramers and reduced microfibril formation as a result of Bethlem myopathy and introduced triple helical glycine mutations. *J. Biol. Chem.* 277:1949–1956.

Leckband, D. 2000. Measuring the forces that control protein interactions. *Annu. Rev. Biophys. Biomol. Struct.* 29:1–26.

Long, J., and P. Chen. 2001. Surface characterization of hydrosilyated polypropylene: contact angle measurement and atomic force microscopy. *Langmuir.* 17:2965–2972.

Luckham, P. F., and J. Klein. 1984. Forces between mica surfaces bearing adsorbed poly-electrolyte poly-L-lysine, in aqueous-media. *J. Chem. Soc. Faraday Trans. 1* 80:865–878.

Morra, M., E. Occhiello, and F. Garbassi. 1990. Knowledge about polymer surfaces from contact angle measurements. *Adv. Colloid Interface Sci.* 32:79–116.

Muller, D. J., M. Amrein, and A. Engel. 1997. Adsorption of biological molecules to a solid support for scanning probe microscopy. *J. Struct. Biol.* 119:172–188.

Neumann, A. W., and R. J. Good. 1972. Thermodynamics of contact angles. I. Heterogeneous solid surfaces. *J. Colloid Interface Sci.* 38:341–358.

Pashley, R. M. 1981. DLVO and hydration forces between mica surfaces in Li^+, Na^+, Na^+ and Cs^+ electrolyte solutions, a correlation of double layer and hydration forces with surface cation exchange properties. *J. Colloid Interface Sci.* 83:531–546.

Raghavachari, M., H.-M. Tsai, K. Kottke-Marchant, and R. E. Marchant. 2000. Surface dependent structures of von Willebrand factor observed by AFM under aqueous conditions. *Colloids Surf. B. Biointerfaces.* 19: 315–324.

Robinson, P. N., and M. Godfrey. 2000. The molecular genetics of Marfan syndrome and related microfibrillopathies. *J. Med. Genet.* 37:9–25.

Rock, M. J., S. A. Cain, L. J. Freeman, A. Morgan, K. T. Mellody, A. Marson, C. A. Shuttleworth, A. S. Weiss, and C. M. Kielty. 2004. Molecular basis of elastic fibre formation: critical interaction and a tropoelastin–fibrillin-1 crosslink. *J. Biol. Chem.* In press.

Schwartz, L. W., and S. Garoff. 1985. Contact angle hysteresis on heterogeneous surfaces. *Langmuir.* 1:219–230.

Sherratt, M. J., C. Baldock, J. L. Haston, D. F. Holmes, C. J. P. Jones, C. A. Shuttleworth, T. J. Wess, and C. M. Kielty. 2003. Fibrillin microfibrils are stiff reinforcing fibres in compliant tissues. *J. Mol. Biol.* 332:183–193.

Sherratt, M. J., D. F. Holmes, C. A. Shuttleworth, and C. M. Kielty. 1997. Scanning transmission electron microscopy mass analysis of fibrillin-containing microfibrils from foetal elastic tissues. *Int. J. Biochem. Cell Biol.* 29:1063–1070.

Sherratt, M. J., T. J. Wess, C. Baldock, J. L. Ashworth, P. P. Purslow, C. A. Shuttleworth, and C. M. Kielty. 2001. Fibrillin-rich microfibrils of the extracellular matrix: ultrastructure and assembly. *Micron* 32:185–200.

Specks, U., U. Mayer, R. Nischt, T. Spissinger, K. Mann, R. Timpl, J. Engel, and M. L. Chu. 1992. Structure of recombinant N-terminal globule of type VI collagen alpha 3 chain and its binding to heparin and hyaluronan. *EMBO J.* 11:4281–4290.

Sweeney, J. B., T. Davis, L. E. Scriven, and J. A. Zasadzinski. 1993. Equilibrium thin films on rough surfaces. 1. Capillary and disjoining effects. *Langmuir.* 9:1551–1555.

Takeda, S., K. Yamamoto, Y. Hayasaka, and K. Matsumoto. 1999. Surface OH group governing wettability of commercial glasses. *J. Non-Cryst. Solids.* 249:41–46.

Trask, B. C., T. M. Trask, T. Broekelmann, and R. P. Mecham. 2000. The microfibrillar proteins MAGP-1 and fibrillin-1 form a ternary complex with the chondroitin sulfate proteoglycan decorin. *Mol. Biol. Cell.* 11: 1499–1507.

Velegol, S. B., and R. D. Tilton. 2001. A connection between interfacial self-assembly and the inhibition of hexadecyltrimethylammonium bromide adsorption on silica by poly-L-lysine. *Langmuir.* 17:219–227.

Wess, T. J., P. P. Purslow, M. J. Sherratt, J. Ashworth, C. A. Shuttleworth, and C. M. Kielty. 1998. Calcium determines the supramolecular organization of fibrillin-rich microfibrils. *J. Cell Biol.* 141:829–837.

Wright, D. W., and R. Mayne. 1988. Vitreous humour of chicken contains 2 fibrillar systems: an analysis of their structures. *J. Ultrastruct. Mol. Struct. Res.* 100:224–234.

Yang, G., K. A. Woodhouse, and C. M. Yip. 2002. Substrate-facilitated assembly of elastin-like peptides: studies by variable-temperature in situ atomic force microscopy. *J. Am. Chem. Soc.* 124:10648–10649.